Journal of Photochemistry and Photobiology A: Chemistry 199 (2008) 112–118

Contents lists available at ScienceDirect

Journal of Photochemistry and Photobiology A: Chemistry

journal homepage: www.elsevier.com/locate/jphotochem

Characterization of the hydroperoxyl/superoxide anion radical ($HO_2^{\bullet}/O_2^{\bullet-}$) formed from the photolysis of immobilized TiO_2 in a continuous flow

Bum Gun Kwon*

Environmental & Whole Information System (E&WIS), #406 Mario Tower, Guro-3-dong, Guro-gu, Seoul 152-848, Republic of Korea

ARTICLE INFO

Article history:
Received 3 July 2007
Received in revised form 25 February 2008
Accepted 8 May 2008
Available online 15 May 2008

Keywords:
Immobilized TiO_2
Hydroperoxyl/superoxide anion radical
Kinetic method
Continuous flow injection

ABSTRACT

In this study, the steady-state concentrations of $HO_2^{\bullet}/O_2^{\bullet-}$ formed from the photocatalysis of immobilized TiO_2 were investigated quantitatively by using the kinetic method with a continuous flow injection. In air-equilibrated water, the concentration of $HO_2^{\bullet}/O_2^{\bullet-}$ was typically 1.01 ($\pm$0.08) $\times 10^{-9}$ M at pH 5.80 in the absence of buffers. The reduction of O_2 by photo-induced electrons (e_{cb}^-) was increased by the concentration of O_2 (from 0 to 0.38 mM). However, in the presence of buffer anions the concentration of $HO_2^{\bullet}/O_2^{\bullet-}$ was gradually decreased by increasing pH. This indicates that the suppression of $HO_2^{\bullet}/O_2^{\bullet-}$ in the presence of buffer ions is attributed to the blocking of active sites of the immobilized TiO_2 photocatalyst and to certain processes, that is, the reaction between $HO_2^{\bullet}/O_2^{\bullet-}$ and $^{\bullet}OH$ (and/or h_{vb}^+). Furthermore, the concentration of $HO_2^{\bullet}/O_2^{\bullet-}$ increased with the increasing concentrations of H_2O_2 and oxalate, and then on the further addition of H_2O_2 (>10 mM) and oxalate (>2 mM), the concentration of $HO_2^{\bullet}/O_2^{\bullet-}$ reached steady values. These results strongly suggest that $HO_2^{\bullet}/O_2^{\bullet-}$ formed on TiO_2 photocatalysis migrates into the water bulk, and this study can contribute significantly to the body of knowledge regarding $HO_2^{\bullet}/O_2^{\bullet-}$ at very low levels.

1. Introduction

Photocatalytic applications of TiO_2 have been of major interest in the area of wastewater treatment, especially when the wastewater contains a wide variety of undesirable pollutants [1–3]. In the previous studies of the TiO_2 photolysis, reactive intermediates such as the hydroxyl radical ($^{\bullet}OH$) [4–13], the hydroperoxyl/superoxide anion radical ($HO_2^{\bullet}/O_2^{\bullet-}$) [12–22], singlet oxygen ($^1O_2$) [17–22], and hydrogen peroxide (H_2O_2) [15,20] have been identified and their formation mechanisms have also been proposed. While the hydroxyl radicals produced on hydrated TiO_2 particles are fairly well investigated in a series of degradation reactions with pollutant molecules [4–13,23,24], much less attention has been paid to the role of $HO_2^{\bullet}/O_2^{\bullet-}$. Recently, several studies have paid much more attention to the behaviors of $HO_2^{\bullet}/O_2^{\bullet-}$ produced through the electron transfer from the TiO_2 surface to dissolved oxygen (O_2), since the formation of $HO_2^{\bullet}/O_2^{\bullet-}$ is important process to determine the efficiency of TiO_2 photocatalytic reactions by means of the decrease of electron–hole (e^-–h^+) recombination [15,16,24]. In view of this point, the physicochemical features on $HO_2^{\bullet}/O_2^{\bullet-}$ formation, i.e., migrated (or drift) $HO_2^{\bullet}/O_2^{\bullet-}$, are very important to explore the TiO_2 photocatalytic activity. In addition, a large amount of attention has been focused on the potential role of $HO_2^{\bullet}/O_2^{\bullet-}$ in eliminating various pollutants in water including atrazine, phenols, and chlorophenol [25–29]. Nevertheless, further investigated is warranted concerning the generation and deactivation of $HO_2^{\bullet}/O_2^{\bullet-}$, as well, quantitative information is needed [15–17,19,24].

Although a number of studies have been conducted to investigate $HO_2^{\bullet}/O_2^{\bullet-}$ formation in the TiO_2 photolysis, the basic mechanism is considered to represent the best reaction model for explaining the fate of $HO_2^{\bullet}/O_2^{\bullet-}$ in an aqueous phase as follows [12,16,30–35]:

$$TiO_2 + h\upsilon (< 400\,nm) \rightarrow h_{vb}^+ + e_{cb}^- \quad (I)$$

$$H_2O\,(or OH^-) + h_{vb}^+ \rightarrow {}^{\bullet}OH + H^+ \quad (II)$$

$$O_2 + e_{cb}^- \rightarrow O_2^{\bullet-} \quad (III)$$

$$O_2^{\bullet-} + H^+ \leftrightarrow HO_2^{\bullet} \quad (IV)$$

$$O_2^{\bullet-} + h_{vb}^+ \rightarrow O_2 \quad (V)$$

In the aqueous phase, the photolysis of TiO_2 leads to the formation of a valence band hole (h_{vb}^+) and a conduction band electron (e_{cb}^-) in reaction (I). The hydroxyl radical ($^{\bullet}OH$) is produced from H_2O (or

* Present address: Biofilm Engineering Laboratory, School of Chemical Engineering, College of Engineering, Seoul National University, San 56-1, Sillim-dong, Gwanak-gu, Seoul 151-742, Republic of Korea. Tel.: +82 2 880 8941; fax: +82 2 876 8911.
E-mail address: kwonbg0@daum.net.

1010-6030/$ – see front matter © 2008 Elsevier B.V. All rights reserved.
doi:10.1016/j.jphotochem.2008.05.001

OH^-) on the hydrated TiO_2 surface by trapping an h_{vb}^+ (reaction (II)). Subsequently, the oxygen molecules adsorbed on the surface of air-saturated TiO_2 act as electron scavengers and combine with e_{cb}^- to form $O_2^{\bullet-}$ in the reaction (III), which is in an acid–base equilibrium (reaction (VI); pK_a ($HO_2^\bullet$) = 4.8 ± 0.1) [36]. The reduction of O_2 by e_{cb}^- (reaction (III)) can exclude the accumulation of the electrons on the TiO_2 particles as well as e^-–h^+ recombination. However, h_{vb}^+ remaining on the TiO_2 surface is reported to eliminate $O_2^{\bullet-}$ (reaction (V)) [32,33]. Thus, the formation of $HO_2^\bullet/O_2^{\bullet-}$ has been considered as an intermediate of the ensuing reactions of free radicals in air-saturated water during the photolysis of TiO_2.

Thus far, several methods have been developed for the detection of $HO_2^\bullet/O_2^{\bullet-}$ formed in illuminated TiO_2 suspensions. For an examination of active species produced on TiO_2 surfaces, the electron paramagnetic resonance (EPR) technique has been most commonly used at a very low temperature or at room temperature [5,12,37,38]. However, the EPR technique has only focused on the detection of $HO_2^\bullet/O_2^{\bullet-}$, rather than on the determination of the absolute concentration of $HO_2^\bullet/O_2^{\bullet-}$. Nosaka et al. [14,15] and Hirakawa et al. [24,33] have recently developed a chemiluminescence (CL) method to detect reactive oxygen species formed on a TiO_2 photocatalyst. They dropped luminol as a specific probe on a TiO_2 aqueous suspension or on TiO_2 film. However, this method has a shortcoming, in that reactions with various reactive oxygen species without the separation of $HO_2^\bullet/O_2^{\bullet-}$ occur; thus only an estimated (or calculated) concentration of $HO_2^\bullet/O_2^{\bullet-}$ is reported. In contrast, Ishibashi et al. [16,19] applied this method using luminol or MCLA (2-methyl-6-(*p*-methoxyphenyl)-3,7-dihydroimidazo-[1,2-*a*]pyrazin-3-one) as a specific probe to TiO_2 film-type photocatalysts in air and in water. To determine the absolute number of $O_2^{\bullet-}$, the photon emission standards were measured from the luminol oxidation initiated with the addition of 0.1% hydrogen peroxide in a standard cell, and the quantitative number of $O_2^{\bullet-}$ was then estimated by comparing the photon number from the standard photon emission of luminol with that emitted from the reaction between photo-generated $O_2^{\bullet-}$ and luminol [19]. However, there are issues with an interfering effect such as H_2O_2-induced CL in the presence of metal and additionally required experimental such as a standard photon emission. Other issues involve the selectivity of luminol from various reactive oxygen species during TiO_2 photolysis [15,19,24,33]. Interestingly, no such steady-state concentration of $HO_2^\bullet/O_2^{\bullet-}$ formed at continuous flow injection has been reported to the best of my knowledge. Thus, information regarding the concentration of $HO_2^\bullet/O_2^{\bullet-}$ has been limited in previous studies involving the photolysis of TiO_2.

For an alternative method of determining the $HO_2^\bullet/O_2^{\bullet-}$ concentration, Kwon et al. [39,40] developed a kinetic method for the measurement of $HO_2^\bullet/O_2^{\bullet-}$ in an aqueous solution. In this method, a calibration procedure using a kinetic half-life technique is established for determining the concentration of $HO_2^\bullet/O_2^{\bullet-}$ as produced in the UV/H_2O_2 process. The kinetic method has shown high sensitivity with a simple calibration system.

In this study, the steady-state concentration of $HO_2^\bullet/O_2^{\bullet-}$ in an illuminated TiO_2 film using the kinetic method is quantitatively determined. To investigate the generation and deactivation of $HO_2^\bullet/O_2^{\bullet-}$ in the photolysis of TiO_2, various effects of the pH using anion buffers, dissolved oxygen, and wavelengths are examined. In addition, the effects of hydrogen peroxide and oxalate are examined in the TiO_2 photolysis. In particular, this study is the first report of utilizing the continuous flow injection in the investigation of TiO_2 photocatalytic reactions on the generation and deactivation of $HO_2^\bullet/O_2^{\bullet-}$ to my knowledge.

2. Experimental

2.1. Materials

Anatase TiO_2 (particle size-325 mesh, 99+%) was obtained from Aldrich. Ferric ethylenediaminetetra acetate (Fe^{3+}-EDTA), sulfuric acid, sodium hydroxide, benzoic acid (BA), sodium oxalate, and 3% H_2O_2 were of reagent grade and were purchased from Sigma–Aldrich. The solution pH was adjusted to the ranges between 5 and 9.5 with a phosphate buffer (Sigma) and a borate buffer (LabChem Inc.) in addition to H_2SO_4 and NaOH. The concentration of the H_2O_2 stock solution was determined through the use of a $KMnO_4$ titration method prior to use. The working H_2O_2 solution was prepared daily by diluting the H_2O_2 stock solution with the proper level with high-purity deionized (DI) water. O_2 saturation in the DI water was achieved by purging high purity O_2 gas (≥99.995%) to dissolve molecular oxygen, and N_2 saturation in the DI water was achieved through the use of high purity N_2 gas (≥99.99%) to remove molecular oxygen. All other chemicals were of analytical grade and were used as received. All solutions were made with high-purity (>18 MΩ cm) DI water from the Younglin ultra-purification system (Korea).

2.2. Preparation of the TiO_2-coated quartz coil

TiO_2 particles were immobilized on the inner surface of a quartz coil (i.d. 1 mm × length 900 mm; inner surface **area ≈2800 mm^2). The quartz coil was pre-cleaned with 1% nitric acid and washed with pumped DI water by pumping for 2 h at 1.00 mL/min. Two hundred micrograms of TiO_2 was added into 3 mL methanol, and this was stirred with a magnetic stirrer. 0.3 mL TiO_2 suspension was gradually poured into the quartz coil and it was dried at 40 °C. This process was repeated 10 times to achieve an even coating. This coil was subsequently calcined in a furnace at 600 °C for 3 h [41]. Following this, the quartz coil with the immobilized TiO_2 particles was cooled to room temperature in air. X-ray diffraction (XRD) was used to analyze the change of crystalline structure of TiO_2. Anatase and rutile TiO_2 were both present in the calcined powders, but the main structure was anatase (data not shown).

2.3. $HO_2^\bullet/O_2^{\bullet-}$ determination in the photolysis of TiO_2

A schematic diagram for the $HO_2^\bullet/O_2^{\bullet-}$ measurement system is shown in Fig. 1. The apparatus and the experimental procedures employed in this study are similar to those of a previous study [39,40] except the TiO_2 particles immobilized on the quartz coil. All solutions were delivered using a peristaltic pump (Ismatec, type ISM 946) with PTFE tubing (Cole-Parmer, i.d. 1.07 mm).

During the measurement of $HO_2^\bullet/O_2^{\bullet-}$, DI water was delivered through Port 1 (P1, 0.43 mL/min) with Valve 1 (V1) opened, while Valve 2 (V2) and Valve 3 (V3) were closed. Dissolved oxygen (DO) in the DI water led to the formation of $HO_2^\bullet/O_2^{\bullet-}$ in the TiO_2-coated quartz coil illuminated with a 4-W low pressure Hg lamp (Sankyo Denki Co., Japan). H_2O_2 was added through Port 2 (P2, 0.23 mL/min) and was mixed with a premixed solution containing Fe^{3+}-EDTA (P3, 0.23 mL/min) and BA (P4, 0.23 mL/min). The Fe^{3+}-EDTA was reduced by $HO_2^\bullet/O_2^{\bullet-}$ to Fe^{2+}-EDTA with $k_6 = 2 \times 10^6\ M^{-1}\ s^{-1}$.

$$Fe^{3+}\text{-EDTA} + O_2^{\bullet-}(HO_2^\bullet) \rightarrow Fe^{2+}\text{-EDTA} + O_2(+H^+) \quad \text{(VI)}$$

A subsequent Fenton-like reaction between Fe^{2+}-EDTA and H_2O_2 ($k_7 = (2 \pm 1) \times 10^4\ M^{-1}\ s^{-1}$) led to the production of the $^\bullet$OH radicals and to the regeneration of Fe^{3+}-EDTA.

$$Fe^{2+}\text{-EDTA} + H_2O_2 \rightarrow Fe^{3+}\text{-EDTA} + OH^- + {}^\bullet OH \quad \text{(VII)}$$

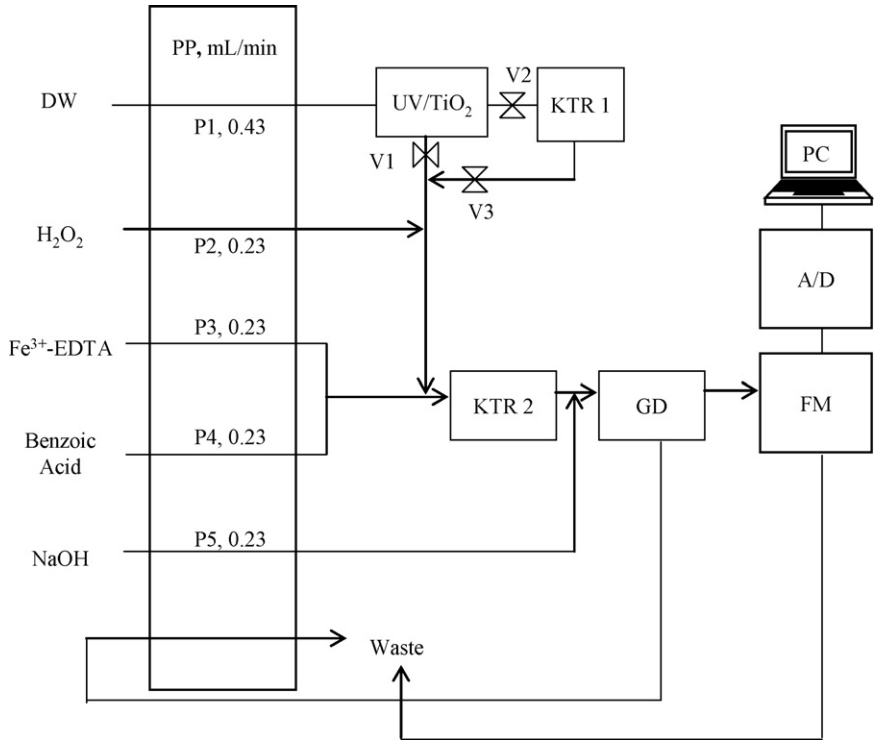

Fig. 1. Schematic diagram and calibration equipment for measuring $HO_2^{\bullet}/O_2^{\bullet-}$. PP, peristaltic pump; P1, P2, P3, P4, and P5, solution inlet ports; UV/TiO_2, UV light and immobilized TiO_2 quartz reactor; V1, V2, and V3, manually operated valves; KTR 1 and KTR 2, knotted tubing reactors; GD, glass debubbler; A/D, A/D converter; FM, fluorometer; PC, computer.

Following this, the $^{\bullet}OH$ radicals produced OHBA in the presence of BA with a nearly diffusion-controlled rate constant of $k_8 = 4.3 \times 10^9\ M^{-1}\ s^{-1}$ in knotted tubing reactor 2 (KTR 2).

$$^{\bullet}OH + BA \rightarrow OHBA \quad \text{(VIII)}$$

0.05N NaOH (P5, 0.23 mL/min) was then added to raise the pH level above 11 at which the fluorescence signal of OHBA could be maintained at a maximum level. The mixed solution occasionally caused the formation of air bubbles in the effluent stream, which was removed by a glass debubbler (GD) prior to the fluorometer (FM) in order to prevent noise signals caused by the air bubbles.

The OHBA fluorescence was then measured with a fluorometer (Waters 474 model) equipped with a 16 μL flow-through cell with $\lambda_{ex} = 320$ nm/$\lambda_{em} = 400$ nm with slit-width of 40 nm. The fluorescence signal was transferred to a data acquisition system, *Auto-chrowin* (Younglin, Korea), consisting of an analog-to-digital converter (A/D) with a personal computer (PC).

2.4. Calibration procedures for $HO_2^{\bullet}/O_2^{\bullet-}$

The calibration procedure employed in this work is described in detail in the previous study [39,40] except for the immobilized TiO_2 particles in the quartz coil as a self-calibration tool. All working solutions containing 4–8 mM H_2O_2, 20–40 μM Fe^{3+}-EDTA, 1 mM benzoic acid (BA), and 0.05N NaOH were passed through the appropriate ports under UV with the lamp-off; as well, the base lines were monitored. During calibration of the $HO_2^{\bullet}/O_2^{\bullet-}$ concentration, V2 and V3 were open, while V1 was closed, as shown in Fig. 1. In the absence of additives, $HO_2^{\bullet}/O_2^{\bullet-}$ in knotted tubing reactor (KTR 1) is disproportionated by the self-reactions according to the empirically observed pH-dependent rate constant, k_{obs} [36]:

$$HO_2^{\bullet} + HO_2^{\bullet} \rightarrow H_2O_2 + O_2 \quad \text{(IX)}$$

$$HO_2^{\bullet} + O_2^{\bullet-} + H_2O \rightarrow H_2O_2 + O_2 + OH^- \quad \text{(X)}$$

$$O_2^{\bullet-} + O_2^{\bullet-} + 2H_2O \rightarrow H_2O_2 + O_2 + 2OH^- \quad \text{(XI)}$$

$$k_{obs} = \frac{k_9 + k_{10}(K_{HO_2}/[H^+])}{(1 + K_{HO_2}/[H^+])^2} \quad (1)$$

where at a given pH k_{obs} can be calculated using $k_9 = (8.3 \pm 0.7) \times 10^5\ M^{-1}\ s^{-1}$, $k_{10} = (9.76 \pm 0.6) \times 10^7\ M^{-1}\ s^{-1}$, $k_{11} < 0.3\ M^{-1}\ s^{-1}$, and $K_{HO_2} = 1.6 \times 10^{-5}\ M^{-1}$ as recommended values [36]. The rate of second-order reaction mainly given by the reactions (IX) and (X) is

$$-\frac{d[HO_2^{\bullet}/O_2^{\bullet-}]}{dt} = k_{obs}\left[HO_2^{\bullet}/O_2^{\bullet-}\right] \quad (2)$$

The solution of Eq. (2) is

$$k_{obs} \times t = \frac{[HO_2^{\bullet}/O_2^{\bullet-}]_o - [HO_2^{\bullet}/O_2^{\bullet-}]_t}{[HO_2^{\bullet}/O_2^{\bullet-}]_o \times [HO_2^{\bullet}/O_2^{\bullet-}]_t} \cong SR = \frac{A_o - A_t}{A_o A_t} \quad (3)$$

The signal ratio (SR) can be defined as $(A_o - A_t)/(A_o \times A_t)$ where A_o is the signal intensity of OHBA at KTR 1 of 0 m and A_t is the signal intensity of OHBA at KTR 1 of 1 m, 2 m, 3 m, and 4 m, respectively. Since $[HO_2^{\bullet}/O_2^{\bullet-}]_{t_{1/2}}$ is equal to $[HO_2^{\bullet}/O_2^{\bullet-}]_o/2$ at the half-life ($t_{1/2}$), Eq. (3) becomes

$$[HO_2^{\bullet}/O_2^{\bullet-}]_o = \frac{1}{k_{obs} \times t_{1/2}} \quad (4)$$

For the second-order reaction, the $t_{1/2}$ is inversely proportional to the initial concentration of $HO_2^{\bullet}/O_2^{\bullet-}$. Thus, the concentration of $HO_2^{\bullet}/O_2^{\bullet-}$ can readily be determined from the $t_{1/2}$ of $HO_2^{\bullet}/O_2^{\bullet-}$ decay in the aqueous solution by calculating k_{obs} at a given pH.

The half-life ($t_{1/2}$) of $HO_2^{\bullet}/O_2^{\bullet-}$ is experimentally measured by plotting the linear relationship of SR vs. the reaction time based on each length of KTR 1. As self-reactions (IX)–(XI) occurred in KTR 1, the concentrations of $HO_2^{\bullet}/O_2^{\bullet-}$ were expected to decrease as the

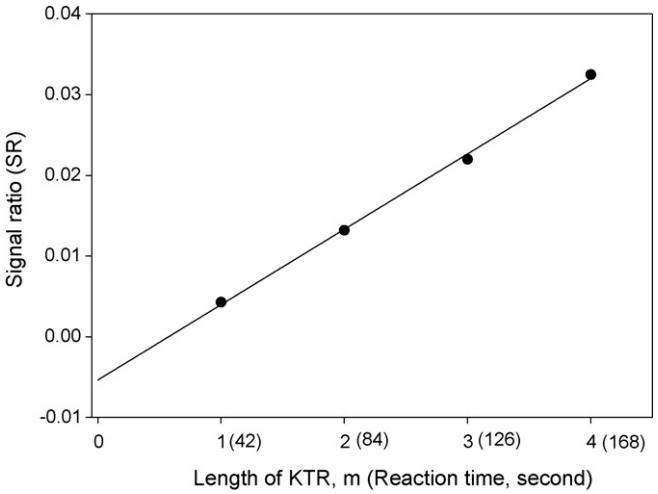

Fig. 2. Plot of SR vs. reaction time with straight line: pH 5.80, λ = 254 nm, [BA] = 1 mM, [H_2O_2] = 4 mM, [Fe^{3+}-EDTA] = 20 μM, and [NaOH] = 0.05N.

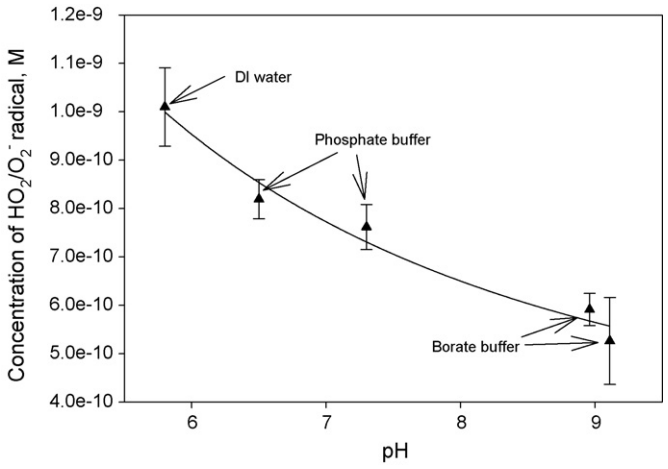

Fig. 3. Dependence of the concentration of $HO_2^{\bullet}/O_2^{\bullet-}$ on increasing of pH in the presence of various buffer ions: λ = 254 nm, [BA] = 1 mM, [H_2O_2] = 4 mM, [Fe^{3+}-EDTA] = 20 μM, [NaOH] = 0.05N, [DO] = 0.194 mM, and KTR = 0 m.

length of KTR 1 increased. These were step-wise, and varied: 0, 1, 2, 3, and 4 m. Hence, the signal intensity of OHBA corresponding to the concentration of $HO_2^{\bullet}/O_2^{\bullet-}$ decreased as the length of KTR 1 increased, and was converted into the reaction time by the constant flow rate through KTR 1 and the constant volumes. A plot of the SR vs. reaction time results in a straight line (Fig. 2) as expected, which produced a pair of slope and intercept at each given pH. From these slopes and intercepts, the half-life ($t_{1/2}$) was derived through the following:

$$SR_{t_{1/2}} = \text{slope} \times t_{1/2} + \text{intercept} \quad (5)$$

Here, $SR_{t_{1/2}}$ is the SR of the half-life, becoming identical with $1/A_o$ at $t_{1/2}$. Consequently, a given concentration of $HO_2^{\bullet}/O_2^{\bullet-}$ was kinetically calculated from Eq. (4), based on the $t_{1/2}$ and calculated k_{obs} at a given pH.

2.5. Measurements of UV light intensity and dissolved oxygen (DO)

The light intensities of UV-C (λ = 254 nm) and UV-A (λ = 365 nm) were measured with ferrioxalate actinometry [42]. The DO was measured with YSI model 58 (USA).

3. Results and discussion

3.1. Effects of the pH and buffer

In the previous studies, Nosaka et al. [15] reported that the concentration of $O_2^{\bullet-}$ was estimated to be approximately 5×10^{-13} M from the CL of luminol dropped on suspended-TiO_2 (15 mg/3.5 mL) during illumination using a 150-W xenon lamp at the wavelength of 387 ± 11 nm and under an alkaline solution of pH 11.5 with 0.01 M NaOH. Hirakawa et al. [33] also reported that the concentration of $O_2^{\bullet-}$ in the same apparatus and experimental procedures as those used by Nosaka et al. [15] was estimated to be about $0.69–0.96 \times 10^{-13}$ M using an alkaline solution of pH 11.5 with 0.01 M NaOH. In addition, Hirakawa et al. [24] experimentally reported again that the concentration of $O_2^{\bullet-}$ using a similar apparatus and experimental procedures, as those of Nosaka et al. [15] and Hirakawa et al. [33], was measured to be approximately 1.2×10^{-6} M using an alkaline solution of pH 11.5 with 0.01 M NaOH, which is inconsistent with the previous results. The cause of the inconsistency may have resulted from the different methods of determining the amount of $O_2^{\bullet-}$. In other words, the results reported by Nosaka et al. [15] and Hirakawa et al. [33] were estimated by calculating a simple model [43], while the concentrations reported by Hirakawa et al. [24] were based on an experimental result using an apparatus factor or a standard CL intensity [44]. As the difference between their results is very large by an order of magnitude of seven under identical experiment, it is necessary to further investigate the precise amount of $O_2^{\bullet-}$ through inter-comparative activities. However, these data are only limited with a strong alkaline solution (pH ≈ 11) as pre-addition or post-addition of probe reagents. The present result shows the steady-state concentrations of $HO_2^{\bullet}/O_2^{\bullet-}$ in a continuous flow under a wider range of pH levels.

Fig. 3 shows that the concentration of $HO_2^{\bullet}/O_2^{\bullet-}$ in the photolysis of immobilized TiO_2 depends significantly on the solution pH. In this experiment, the solution pH levels were held in a range from 5.6 to 9.1 through the use of phosphate and borate in addition to NaOH. In the presence of buffers, the concentration of $HO_2^{\bullet}/O_2^{\bullet-}$ decreased as the pH increased, ranging from $1.01 (\pm 0.08) \times 10^{-9}$ M (pH 5.6, air-equilibrated DI water) to $0.53 (\pm 0.09) \times 10^{-9}$ M (pH 9.1 using borate buffer and NaOH). The concentration of $HO_2^{\bullet}/O_2^{\bullet-}$ formed at pH 5.6 is nearly twice as high as that of $HO_2^{\bullet}/O_2^{\bullet-}$ formed at pH 9.1. This result indicates that added buffers influence the formation process of $HO_2^{\bullet}/O_2^{\bullet-}$ in the photolysis of immobilized TiO_2.

According to Eq. (1), $HO_2^{\bullet}/O_2^{\bullet-}$ at pH 4.8 ($pK_{HO_2^{\bullet}}$) disappears with the highest disproportionation rate, while it slowly disappears as the pH increases [36]. Hence, the concentration of $HO_2^{\bullet}/O_2^{\bullet-}$ at pH 5.6 should be lower than that of $HO_2^{\bullet}/O_2^{\bullet-}$ at pH 9.1 under identical concentrations of $HO_2^{\bullet}/O_2^{\bullet-}$. However, such a trend was not observed in the presence of buffer ions as shown in Fig. 3. One possible explanation for this result is that the TiO_2 surface caused by illumination immediately becomes more positively charged [45], indicating that the anionic buffer ions can be adsorbed onto the illuminated TiO_2 surface. Even though before illumination the anionic buffer ions cannot be adsorbed easily on the negative TiO_2 surface at pH > 7 owing to electrostatic repulsion [46,47], it was experimentally demonstrated that the surface of TiO_2 particles always shifted to more positive values during illumination, irrespective of the initial pH values [45]. For this reason, the available adsorbed O_2 at the air-saturated TiO_2 surface during illumination can be decreased by adsorbed buffer ions on the TiO_2 surface, which impedes the electron transfer to O_2 producing $HO_2^{\bullet}/O_2^{\bullet-}$ through the reaction (III).

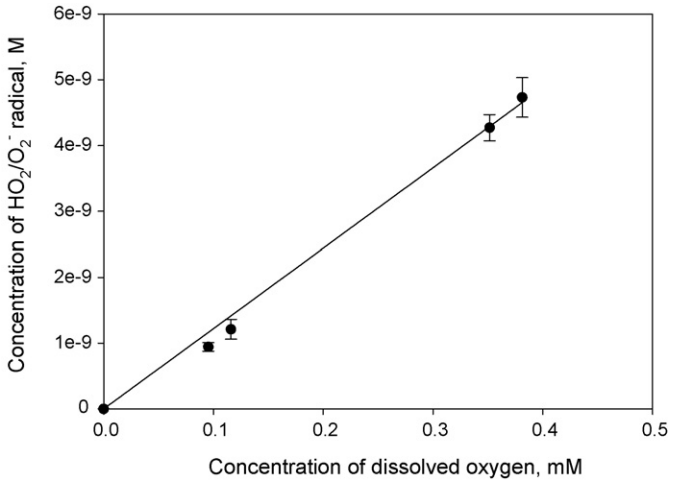

Fig. 4. Dependence of the steady-state concentration of $HO_2^{\bullet}/O_2^{\bullet-}$ on DO concentration depending on both initial aerated and deaerated conditions: pH 5.80, λ = 254 nm, [BA] = 1 mM, [H_2O_2] = 4 mM, [Fe^{3+}-EDTA] = 20 μM, and [NaOH] = 0.05N.

Another possible explanation for this experimental result is that the decay of $HO_2^{\bullet}/O_2^{\bullet-}$ formed over the heterogeneous surface of the TiO_2 particles may be caused by the rapid reactions (XII) and (XIII) [48] and by the reaction (V) [24].

$$O_2^{\bullet-} + {}^{\bullet}OH \rightarrow O_2 + OH^- \quad \text{(XII)}$$

$$HO_2^{\bullet} + {}^{\bullet}OH \rightarrow O_2 + 2H_2O \quad \text{(XIII)}$$

In addition, no reactions of buffer ions, i.e., borate and/or phosphate ions, with e_{cb}^- and/or h_{vb}^+ was reported so far, and the $HO_2^{\bullet}/O_2^{\bullet-}$ was mostly unreactive toward buffer ions (<0.02 M^{-1} s^{-1}) [36,48]. Thus, the suppression of $HO_2^{\bullet}/O_2^{\bullet-}$ in the presence of buffer ions is attributed to the blocking of active sites of the immobilized TiO_2 photocatalyst and to certain processes, that is, the reaction between $HO_2^{\bullet}/O_2^{\bullet-}$ and $^{\bullet}OH$ (and/or h_{vb}^+).

3.2. Effects of oxygen

Although Nosaka et al. [15] and Hirakawa et al. [24,33] reported a concentration of $O_2^{\bullet-}$ in their studies using a luminol CL technique, they did not show a measured concentration of $O_2^{\bullet-}$ under O_2- and N_2-saturated conditions or acidic and/or neutral pHs. Furthermore, they indicated that the CL from luminol dropped on each suspended-TiO_2 can be influenced by interfering effects with another adsorbed species or the trapped h_{vb}^+ (or h_{tr}^+) over the heterogeneous surface of the TiO_2 particle [14–16,19,24,33]. The present result shows the steady-state concentrations of $HO_2^{\bullet}/O_2^{\bullet-}$ on the effects of dissolved O_2 under acidic condition in the photolysis of immobilized TiO_2.

Fig. 4 (data in Table 1) shows the O_2-dependence of the $HO_2^{\bullet}/O_2^{\bullet-}$ concentration on the photolysis of immobilized TiO_2 at pH 5.80 (pure DI water) without buffer ions and λ = 254 nm under three different experimental conditions: air-equilibrated, O_2-saturated, and N_2-saturated. The differing conditions for air equilibrium and for O_2 saturation were achieved by mechanical mixing and oxygen gas sparging for 30 min, in which O_2 concentrations were measured in the ranges of 0.11 (±0.01) mM to 0.38 (±0.03) mM (see Table 1). The N_2 saturation for comparison was achieved by nitrogen sparging for 30 min to remove dissolved O_2.

Table 1
Dependence of the concentration of $HO_2^{\bullet}/O_2^{\bullet-}$ generated in the photolysis of immobilized TiO_2 particles as function of O_2 concentration[a]

$[DO]_o$ (mM)	Concentration of $HO_2/O_2^{\bullet-}$ (M)	Standard deviation (±)
0	–	–
0.10 (±0.01)	0.94×10^{-9}	0.65×10^{-10}
0.12 (±0.01)	1.21×10^{-9}	1.5×10^{-10}
0.35 (±0.01)	4.27×10^{-9}	2.0×10^{-10}
0.38 (±0.03)	4.73×10^{-9}	3.0×10^{-10}

[a] All data for Fig. 5.

As shown in Fig. 4, the concentrations of $HO_2^{\bullet}/O_2^{\bullet-}$ generated during the illumination of TiO_2 increase as the dissolved O_2 concentration increases, which shows a reasonable linearity within the experimental error. The concentrations of $HO_2^{\bullet}/O_2^{\bullet-}$ are 1.21 (±0.15) × 10^{-9} M at air equilibrium and 4.73 (±0.31) × 10^{-9} M at O_2 saturation, respectively. In contrast, no measurable signal on the $HO_2^{\bullet}/O_2^{\bullet-}$ formation in the N_2-saturated condition is shown. This result indicates that additional available dissolved O_2 scavenges a greater amount of e_{cb}^- while reducing the chance of the charged pair recombination (h_{vb}^+–e_{cb}^-) [30]. It is evident that the concentration of $HO_2^{\bullet}/O_2^{\bullet-}$ increases as the O_2 concentration increases. Consequently, the present result shows the quantitatively measured concentration of $O_2^{\bullet-}$ depending on O_2 concentrations over the aqueous bulk solution during the illumination of immobilized TiO_2 particles.

3.3. Effects of wavelengths

The effect of the wavelength on the concentration of $HO_2^{\bullet}/O_2^{\bullet-}$ was examined through the photolysis of immobilized TiO_2 particles. This experiment was conducted at pH 5.8 without buffer ions under air-equilibrated condition. The concentration of $HO_2^{\bullet}/O_2^{\bullet-}$ in the photolysis of immobilized TiO_2 shows the dependence of the wavelength (data not shown). The concentration ($1.02 \pm 0.10 \times 10^{-9}$ M) of $HO_2^{\bullet}/O_2^{\bullet-}$ at λ = 254 nm is approximately three times higher than that ($0.37 \pm 0.05 \times 10^{-9}$ M) of $HO_2^{\bullet}/O_2^{\bullet-}$ at λ = 365 nm. This dependence follows the absorption spectrum of TiO_2 as a function of the wavelength, with a threshold corresponding to the band gap energy (>3.2 eV) of the wavelength (≤387 nm) [1–3]. TiO_2 generally shows a strong absorbance at measurements approximately below 300 nm, and thereafter the absorbance of TiO_2 is decreased [9,49]. In this study, the light intensities of 254 and 365 nm in the absence of immobilized TiO_2 were measured with a quintuplicate average to be 3.27 (±0.25) × 10^{-5} Einstein/L s and 1.55 (±0.29) × 10^{-5} Einstein/L s, respectively. Consequently, the light intensity corresponding to absorbance on the immobilized TiO_2 is reduced by increasing wavelength, and then the concentrations of the $HO_2^{\bullet}/O_2^{\bullet-}$ are decreased.

3.4. Effects of H_2O_2

In previous study, Hirakawa et al. [24] has reported that the concentration of $O_2^{\bullet-}$ was measured by the CL method from luminol dropped on each suspended-TiO_2 in the presence of H_2O_2 (<0.4 mM) under an alkaline pH of 11.5. They observed that the concentration of $O_2^{\bullet-}$ was approximately max. 3.35×10^{-6} M at 0.2 mM H_2O_2, and on a further addition of H_2O_2, the concentration of $O_2^{\bullet-}$ decreased and then reached a steady value of nearly 2.3×10^{-6} M at 0.4 mM H_2O_2. Nevertheless, those studies were suggested that the CL method using luminol could be influenced by interfering effects with other adsorbed species or by the trapped h_{vb}^+ (h_{tr}^+) over the heterogeneous surface of the TiO_2 particle [24]. However, the result of the present study is different from those of Hirakawa et al. [24].

Fig. 5 shows a plot for the steady-state concentration of $HO_2^{\bullet}/O_2^{\bullet-}$ as a function of the concentration of H_2O_2. The effect of H_2O_2 (pK_a = 11.7) [15] was investigated at λ = 254 nm and pH 5.6 without buffer ions. As shown in Fig. 5, the concentration

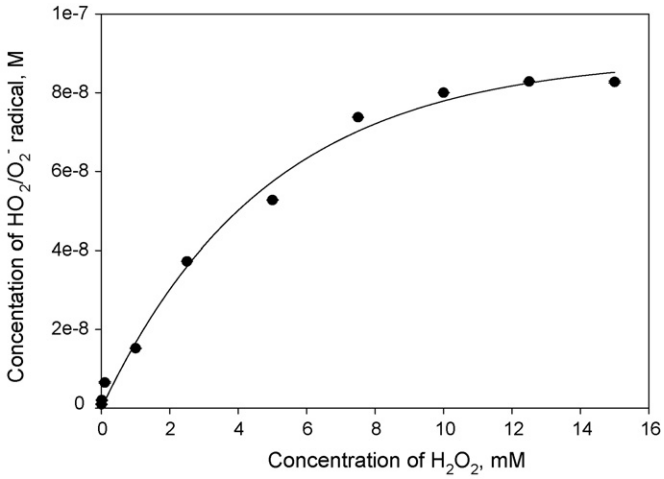

Fig. 5. Dependence of the concentration of $HO_2^{\bullet}/O_2^{\bullet-}$ on increasing H_2O_2 concentration with air-equilibrated system: pH 5.8, λ = 254 nm, [BA] = 1 mM, [H_2O_2] = 4 mM, [Fe^{3+}-EDTA] = 20 μM, [NaOH] = 0.05N, [DO] = 0.194 mM, and KTR = 0 m.

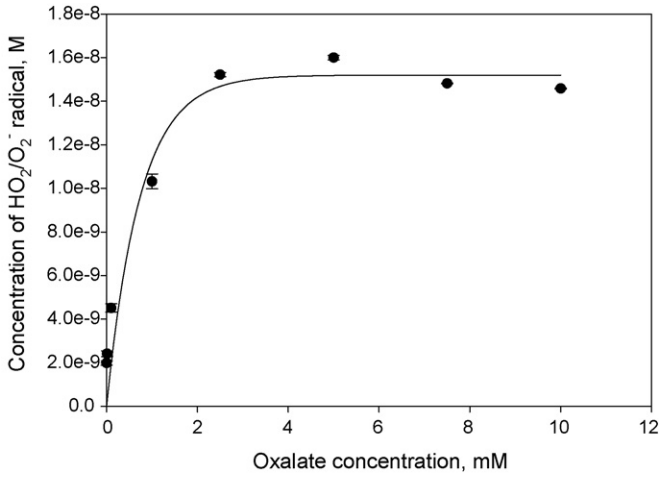

Fig. 6. Dependence of the concentration of $HO_2^{\bullet}/O_2^{\bullet-}$ on increasing oxalate concentration: pH 5.8, λ = 254 nm, [BA] = 1 mM, [H_2O_2] = 4 mM, [Fe^{3+}-EDTA] = 20 μM, [NaOH] = 0.05N, [DO] = 0.194 mM, and KTR = 0 m.

of $HO_2^{\bullet}/O_2^{\bullet-}$ linearly increases as the concentration of H_2O_2 increases at the initial phase, gradually reaching a constant value at about 10 mM H_2O_2. This increase of the $HO_2^{\bullet}/O_2^{\bullet-}$ concentration is attributable to the reactions as follows [9,24,36,48]:

$$H_2O_2 + e_{cb}^- \rightarrow {}^{\bullet}OH + OH^- \quad \text{(XIV)}$$

$$H_2O_2 + {}^{\bullet}OH \rightarrow HO_2^{\bullet} + H_2O \quad \text{(XV)}$$

As the molecular ratio $[HO_2^-]/[H_2O_2]$ is 1.58×10^{-6} in the acidic aqueous solution of pH 5.6, HO_2^- is likely to be negligible in our study. Although H_2O_2 at λ = 254 nm is photo-decomposed to produce •OH [39], the direct decomposition of H_2O_2 at λ = 254 nm may be negligible due to that the immobilization of TiO_2 particles on the inner surface of the quartz coil blocks the light. Hence, H_2O_2 reacts with e_{cb}^- to produce •OH (reaction (XIV), $k_{14} = 1.1 \times 10^{10}\ M^{-1}\ s^{-1}$) [48]. Since the surface-bound OH radicals are unlikely to migrate far from the TiO_2 surface [19,34], most of the OH radicals at the surface of TiO_2 react with H_2O_2 to produce $HO_2^{\bullet}$ (reaction (XV), $k_{15} = 2.7 \times 10^7\ M^{-1}\ s^{-1}$) [48]. However, H_2O_2 to form $HO_2^{\bullet}/O_2^{\bullet-}$ at low H_2O_2 concentration would be competed with O_2 (~0.11 mM) in terms of e_{cb}^-. This is shown in Table 2, in which, with the addition of 0.1 mM H_2O_2, the concentration of $HO_2^{\bullet}/O_2^{\bullet-}$ in the absence of O_2 is lower by approximately 27 times than that of $HO_2^{\bullet}/O_2^{\bullet-}$ in the presence of O_2. Considering the kinetic ratio (=1.9) of k_3([O_2] = 0.11 mM) to k_{14}([H_2O_2] = 0.10 mM), approximately 66% of e_{cb}^- reacts with O_2, whereas approximately 34% of e_{cb}^- reacts with H_2O_2. Thus, reaction (III) ($O_2 + e_{cb}^-$) is dominant at a low concentration of H_2O_2. However, based on the kinetic ratio as mentioned above, 50% of e_{cb}^- at 0.19 mM H_2O_2 can react with H_2O_2. With increasing H_2O_2 (>0.19 mM), the reaction (XIV) ($H_2O_2 + e_{cb}^-$) is gradually dominant, and then most of the •OH radicals generated at the surface of TiO_2 react with H_2O_2 to produce $HO_2^{\bullet}$ (reaction (XV)). Furthermore, after adding 1 mM H_2O_2 the concentration of $HO_2^{\bullet}/O_2^{\bullet-}$ under N_2 purging is similar to that of $HO_2^{\bullet}/O_2^{\bullet-}$ in the air equilibrium as shown in Table 2. From these observations, H_2O_2 mainly serves as an e_{cb}^- acceptor that produces further $HO_2^{\bullet}/O_2^{\bullet-}$ concentration.

3.5. Effect of oxalate

Fig. 6 shows a plot for the concentration of $HO_2^{\bullet}/O_2^{\bullet-}$ as a function of the concentration of oxalate in the photolysis of immobilized TiO_2. The effect of oxalate was examined at λ = 254 nm and pH 5.6 controlled with a small NaOH. As shown in Fig. 6, the concentration of $HO_2^{\bullet}/O_2^{\bullet-}$ linearly increases as the concentration of oxalate at initial step increases. It then reaches its maximum value of 2 mM oxalate. The increase in the $HO_2^{\bullet}/O_2^{\bullet-}$ concentration as the amount of oxalate increases is attributable to the oxidation of $(COO)_2^{2-}$ by h_{vb}^+, as described by the following reactions [50,51]:

$$(COO)_2^{2-} + h_{vb}^+ \rightarrow {}^-OOC\text{–}COO^{\bullet} \quad \text{(XVI)}$$

$${}^-OOC\text{–}COO^{\bullet}{}_2 \rightarrow CO_2^{\bullet-} + CO_2 \quad \text{(XVII)}$$

$$CO_2^{\bullet-} + O_2 \rightarrow O_2^{\bullet-} + CO_2 \quad \text{(XVIII)}$$

$$e_{cb}^- + O_2 \rightarrow O_2^{\bullet-} \quad \text{(XIX)}$$

Oxalate (pK_{a1} = 1.23 and pK_{a2} = 4.19) [52], which is adsorbed onto the positively charged TiO_2 surface at pH 5.6, is directly oxidized by h_{vb}^+ (reaction (XVI)) [50,53]. In the valence band, the h_{vb}^+-mediated oxidation of oxalate leads to the formation of $HO_2^{\bullet}/O_2^{\bullet-}$ with the involvement of O_2. As the molecular ratio $\{(COO)_2^{2-}\}/\{COOH\text{–}(COO)^-\}$ is 0.96 in the acidic solution of pH 5.6, the effect of COOH-$(COO)^-$ is likely to be negligible in the present study. Subsequently, the $^-OOC\text{–}COO^{\bullet}$ radical decomposes

Table 2
Effects of H_2O_2 addition depending on the presence and absence O_2 in the photolysis of immobilized TiO_2 particles

Condition	$[HO_2/O_2^{\bullet-}]$ (M)		
	TiO_2/UV/H_2O_2 at air equilibrium[a]	TiO_2/UV/H_2O_2 at N_2 purging[b]	UV/H_2O_2 at air equilibrium[c]
pH 5.6; [H_2O_2] = 0.1 mM	6.51×10^{-9}	2.45×10^{-10}	–
pH 5.6; [H_2O_2] = 1 mM	1.52×10^{-8}	1.48×10^{-8}	–
pH 6.11; [H_2O_2] = 4 mM	–	–	5.19×10^{-9}

[a] [DO] = 0.1–0.12 mM.
[b] [DO] ≈ 0 mM.
[c] Ref. [39].

into the $CO_2^{\bullet-}$ radical (reaction (XVII)). Following this, $CO_2^{\bullet-}$ radical reacts with residual O_2 ($k_{18} = 2–4.2 \times 10^9\ M^{-1}\ s^{-1}$) [54], giving $O_2^{\bullet-}$. Although a conduction band electron, e_{cb}^-, competes with O_2, $O_2^{\bullet-}$ formed by reaction (III) is a minor portion and can thus be considered insignificant. As oxalate has negligible reactivity with $HO_2^{\bullet}/O_2^{\bullet-}$, $k = 0.2\ M^{-1}\ s^{-1}$ [36], the concentration of $HO_2^{\bullet}/O_2^{\bullet-}$ with the addition of 2 mM oxalate is nearly 10 times higher than that of $HO_2^{\bullet}/O_2^{\bullet-}$ in the absence of oxalate. This result has not been studied thus far. Consequently, the addition of oxalate as a hole scavenger increases the concentration of $HO_2^{\bullet}/O_2^{\bullet-}$ in the photolysis of immobilized TiO_2.

4. Conclusions

In this study, the steady-state concentrations of $HO_2^{\bullet}/O_2^{\bullet-}$ formed from the photocatalysis of immobilized TiO_2 were investigated newly over various factors by using the kinetic method with a continuous flow injection. The concentration of $HO_2^{\bullet}/O_2^{\bullet-}$ increased as the O_2 concentrations increased in the absence of buffers. This indicates that, during photocatalytic reactions, photo-generated electron is mainly trapped by adsorbed oxygen molecules resulting in the formation of $HO_2^{\bullet}/O_2^{\bullet-}$. However, the concentration of $HO_2^{\bullet}/O_2^{\bullet-}$ gradually decreased as the pH increased in the presence of buffers, which was restricted by the available photo-active sites on the immobilized TiO_2 surface. Furthermore, the concentration of $HO_2^{\bullet}/O_2^{\bullet-}$ increased with the increasing concentrations of H_2O_2 and oxalate, and then on the further addition of H_2O_2 (>10 mM) and oxalate (>2 mM), the concentration of $HO_2^{\bullet}/O_2^{\bullet-}$ reached steady values. These results show that $HO_2^{\bullet}/O_2^{\bullet-}$ formed on TiO_2 photocatalysis migrates into the water bulk.

Acknowledgement

This subject is supported by Korea Ministry of Environment as "The Eco-technopia 21 project."

References

[1] M.R. Hoffmann, S.T. Martin, W. Choi, D.W. Bahnemann, Chem. Rev. 95 (1995) 69.
[2] A. Mills, S.L. Hunte, J. Photochem. Photobiol. A 108 (1997) 1.
[3] A.L. Linsebigler, G. Lu, J.T. Yates Jr., Chem. Rev. 95 (1995) 735.
[4] H. Van Damme, W. Keith Hall, J. Am. Chem. Soc. 101 (1979) 4373.
[5] C.D. Jaeger, A.J. Bard, J. Phys. Chem. 83 (1979) 3146.
[6] M. Anpo, T. Shima, S. Kodama, Y. Kubokawa, J. Phys. Chem. 91 (1987) 4305.
[7] J. Cunningham, G. Al-Sayyed, J. Chem. Soc., Faraday Trans. 86 (1990) 3935.
[8] D. Lawless, N. Serpone, D. Meisel, J. Phys. Chem. 95 (1991) 5166.
[9] L. Sun, J.R. Bolton, J. Phys. Chem. 100 (1996) 4127.
[10] P.F. Schwarz, N.J. Turro, S.H. Bossmann, A.M. Braun, A.A. Abdel Wahab, H. Dűrr, J. Phys. Chem. B 101 (1997) 7127.
[11] A.V. Taborda, M.A. Brusa, A. Grela, Appl. Catal. A: General 208 (2001) 419.
[12] R.F. Howe, M. Grätzel, J. Phys. Chem. 91 (1987) 3906.
[13] Y. Nosaka, K. Koenuma, K. Ushida, A. Kira, Langmuir 12 (1996) 736.
[14] Y. Nosaka, H. Fukuyama, Chem. Lett. 383 (1997).
[15] Y. Nosaka, Y. Yamashita, H. Fukuyama, J. Phys. Chem. B 101 (1997) 5822.
[16] K.-I. Ishibashi, Y. Nosaka, K. Hashimoto, A. Fujishima, J. Phys. Chem. B 102 (1998) 2117.
[17] R. Konaka, E. Kasahara, W.C. Dunlap, Y. Yamamoto, K.C. Chien, M. Inoue, Free Radic. Biol. Med. 27 (1999) 294.
[18] T. Tatsuma, S.-I. Tachibana, T. Miwa, D.A. Tryk, A. Fujishima, J. Phys. Chem. B 103 (1999) 8033.
[19] K.-I. Ishibashi, A. Fujishima, T. Watanabe, K. Hashimoto, J. Phys. Chem. B 104 (2000) 4934.
[20] T. Tatsuma, S.-I. Tachibana, A. Fujishima, J. Phys. Chem. B 105 (2001) 6987.
[21] S. Xu, J. Shen, S. Chen, M. Zhang, T. Shen, J. Photochem. Photobiol. B 67 (2002) 64.
[22] T.A. Konovalova, J. Lawrence, L.D. Kispert, J. Photochem. Photobiol. A 162 (2004) 1.
[23] C. Kormann, D.W. Bahnemann, M.R. Hoffmann, Environ. Sci. Technol. 25 (1991) 494.
[24] T. Hirakawa, Y. Nosaka, Langmuir 18 (2002) 3247.
[25] D. Chatterjee, A. Mahata, Appl. Catal. B: Environ. 33 (2001) 119.
[26] D. Chatterjee, A. Mahata, J. Photochem. Photobiol. A 153 (2002) 199.
[27] D. Chatterjee, A. Mahata, J. Photochem. Photobiol. A 165 (2004) 19.
[28] P. Raja, A. Bozzi, H. Mansilla, J. Kiwi, J. Photochem. Photobiol. A 169 (2004)269.
[29] G. Lu, A. Linsebigler, J.T. Yates Jr., J. Phys. Chem. 99 (1995) 7626.
[30] H. Gerisher, A. Heller, J. Phys. Chem. 95 (1991) 5261.
[31] C.-M. Wang, A. Heller, H. Gerischer, J. Am. Chem. Soc. 114 (1992) 5230.
[32] J. Fan, J.T. Yates Jr., J. Am. Chem. Soc. 118 (1996) 4686.
[33] T. Hirakawa, H. Kominami, B. Ohtani, Y. Nosaka, J. Phys. Chem. B 105 (2001) 6993.
[34] S. Upadhya, D.F. Ollis, J. Phys. Chem. B 101 (1997) 2625.
[35] H. Courbon, M. Formenti, P. Pichat, J. Phys. Chem. 81 (1977) 550.
[36] B.H.J. Bielski, D.E. Cabelli, R.L. Arudi, A.B. Ross, J. Phys. Chem. Ref. Data 14 (1985).
[37] J.M. Coronado, A.J. Maira, A. Martínez-Arias, J.C. Conesa, J. Soria, J. Photochem. Photobiol. A 150 (2002) 213.
[38] J. Yu, J. Chen, C. Li, X. Wang, B. Zhang, H. Ding, J. Phys. Chem. B 108 (2004) 2781.
[39] B.G. Kwon, J.H. Lee, Anal. Chem. 76 (2004) 6359.
[40] B.G. Kwon, J.H. Lee, Bull. Korean Chem. Soc. 27 (2006) 1785.
[41] Y. Zhu, L. Zhang, C. Gao, L. Cao, J. Mater. Sci. 35 (2000) 4049.
[42] C.G. Hatchard, C.A. Parker, Proc. R. Soc. A235 (1956) 518.
[43] Luminol CL reactions observed by Nosaka et al. [15] and Hirakawa et al. [33] involve the following two reactions, (R1) and (R2), where $L^{\bullet-}$ and L are luminol radical and two-electron-oxidized luminol, respectively. (R1) $O_2^{\bullet-} + L^{\bullet-} + H^+ \rightarrow LO_2H^- \rightarrow AP^*$; (R2) $HO_2^- + L \rightarrow LO_2H^- \rightarrow AP^*$; The reaction product, LO_2H^-, rapidly decomposes into the excited state of 2-aminophthalate (AP^*) which emits the light at around 425 nm. Since the CL intensity is proportional to the formation rate of LO_2H^-, it is proportional to the concentration products $[O_2^{\bullet-}][L^{\bullet-}]$ and $[HO_2^-][L]$ for (R1) and (R2), respectively. Both reactions contribute to the total CL intensity as expressed by the following Eq. (1), where k_{R1} and k_{R2} are the rate constants of the corresponding reactions and Φ is the quantum yield for (R2). (Eq. (1)) $d[AP^*]/dt = k_{R1}[O_2^{\bullet-}][L^{\bullet-}] + \Phi k_{R2}[HO_2^-][L]$; Thus, from the Eq. (1) amount of $O_2^{\bullet-}$ can be estimated. The details of the analysis method have been described in the previous papers [15,33].
[44] In the luminol CL method, the apparatus factor or a standard CL intensity is required because a large amount of L produced by photocatalytic oxidation of luminol reacts with OH^- ions at pH 11.0 and then emits the visible light. Thus, the concentration of $O_2^{\bullet-}$ can be estimated by comparing the CL intensity from the apparatus factor or a standard CL intensity with that emitted from the reaction between photo-generated $O_2^{\bullet-}$ and luminol [16,19].
[45] J. Zhao, H. Hidaka, A. Takamura, E. Pelizzetti, N. Serpone, Langmuir 9 (1993) 1646.
[46] M. Abdullah, G.K.-C. Low, R.W. Mattews, J. Phys. Chem. 94 (1990) 6820.
[47] G.A. Parks, Chem. Rev. 65 (1965) 177.
[48] G.V. Buxton, C.L. Greenstock, W.P. Helman, A.B. Ross, J. Phys. Chem. Ref. Data 17 (1988).
[49] M. Anpo, Catal. Surv. Jpn. 1 (1997) 169.
[50] Y. Mao, C. Schöneich, K.-D. Asmus, J. Phys. Chem. 95 (1991) 10080.
[51] A.J. Hoffmann, E.R. Carraway, M.R. Hoffmann, Environ. Sci. Technol. 28 (1994) 776.
[52] CRC Handbook of Chemistry and Physics, Editor-in-Chief: David R. Lide, Ph.D. (Former Director, Standard Reference Data National Institute of Standards and Technology), 80th Edition (1999) 8–46.
[53] E.R. Carraway, A.J. Hoffman, M.R. Hoffman, Environ. Sci. Technol. 28 (1994) 786.
[54] P. Neta, R.E. Huie, A.B. Ross, J. Phys. Chem. Ref. Data 17 (1988) 1050.